Transient vibration and product formation of photoexcited CS$_2$ measured by time-resolved X-ray scattering

Ian Gabalski,[1,2] Malick Sere,[1,3] Kyle Acheson,[4] Felix Allum,[1,5] Sébastien Boutet,[5] Gopal Dixit,[6] Ruaridh Forbes,[1,5] James M. Glownia,[5] Nathan Goff,[7] Kareem Hegazy,[1,8] Andrew J. Howard,[1,2] Mengning Liang,[5] Michael P. Minitti,[5] Russell S. Minns,[9] Adi Natan,[1] Nolan Peard,[2] Weronika O. Rasmus,[9] Roseanne J. Sension,[10] Matthew R. Ware,[1] Peter M. Weber,[7] Nicholas Werby,[1,8] Thomas J. A. Wolf,[1,5] Adam Kirrander,[4] and Philip H. Bucksbaum[1,2,8]

[1)] *Stanford PULSE Institute, SLAC National Accelerator Laboratory, Menlo Park, CA 94025, USA*

[2)] *Department of Applied Physics, Stanford University, Stanford, CA 94305, USA*

[3)] *Department of Electrical Engineering, Stanford University, Stanford, CA 94305, USA*

[4)] *School of Chemistry, University of Edinburgh, Edinburgh EH8 9YL, UK*

[5)] *Linac Coherent Light Source, SLAC National Accelerator Laboratory, Menlo Park, CA 94025, USA*

[6)] *Department of Physics, Indian Institute of Technology Bombay, Powai, Mumbai, 400076, India*

[7)] *Department of Chemistry, Brown University, Providence, RI, 02912, USA*

[8)] *Department of Physics, Stanford University, Stanford, CA 94305, USA*

[9)] *School of Chemistry, University of Southampton, Highfield, Southampton SO17 1BJ, UK*

[10)] *Department of Chemistry, University of Michigan, Ann Arbor, MI, 48109, USA*

(Dated: 23 September 2022)

We have observed details of the internal motion and dissociation channels in photoexcited carbon disulfide (CS$_2$) using time-resolved X-ray scattering (TRXS). Photoexcitation of gas-phase CS$_2$ with a 200 nm laser pulse launches oscillatory bending and stretching motion leading to dissociation of atomic sulfur in under a picosecond. During the first 300 fs following excitation we observe significant changes in the vibrational frequency as well as some dissociation of the C-S bond leading to atomic sulfur in the both ^{1}D and ^{3}P states. Beyond 1400 fs the dissociation is consistent with primarily ^{3}P atomic sulfur dissociation. This channel-resolved measurement of the dissociation time is based on our analysis of the time-windowed dissociation radial velocity distribution, which is measured using the temporal Fourier transform of the TRXS data aided by a Hough transform that extracts the slopes of linear features in an image. The relative strength of the two dissociation channels reflects both their branching ratio and differences in the spread of their dissociation times. Measuring the time-resolved dissociation radial velocity distribution aids the resolution of discrepancies between models for dissociation proposed by prior photoelectron spectroscopy work.

I. INTRODUCTION

The interplay between nuclear motion and electronic character in photoexcited molecules continues to challenge our understanding of the dynamics governing chemical reactions. The Born-Oppenheimer approximation makes use of the separation of timescales for electronic and nuclear motion to obtain effective equations of motion for the nuclei and electrons separate from one another. This approximation breaks down, however, in the presence of nonadiabatic or spin-orbit coupling. Such additional coupling terms induce changes in electronic state via spin-allowed internal conversion (IC) and spin-forbidden intersystem crossing (ISC)[1–4]. These effects are of critical importance in photochemistry and photophysics, governing product formation and branching ratios[5–7] as well as providing the mechanism for ultrafast electronic relaxation in molecules[8,9].

Carbon disulfide (CS$_2$) is a triatomic molecule that is linear in the ground state equilibrium geometry. Despite its structural simplicity it is an important model system for studying complex non-Born-Oppenheimer dynamics in chemical reactions. Immediately following 200 nm photoexcitation, CS$_2$ undergoes coupled bending and stretching motions followed by IC and ISC processes

that lead to dissociation of both singlet and triplet atomic sulfur. This vibrational mode coupling is essential to the molecule achieving its observed singlet/triplet product ratio as well as the observed lifetimes of the intermediate states[10–17]. It was suggested in Ref.[11] that the rapid bending and stretching facilitate IC to states with high barriers to dissociation, preventing singlet dissociation after 200 fs while allowing triplet production via ISC to proceed. More recent work has disagreed, suggesting the reaction proceeds through a single intermediate state[18]. Understanding the vibrational mode coupling that occurs leading to these two distinct product states is therefore crucial to building a complete picture of the reaction.

Experimental techniques used to study this CS$_2$ reaction cover a wide range. Photoelectron spectroscopies[11,12,14,18–21] are generally sensitive to the instantaneous electronic state of the system. Ion momentum imaging with state-selective resonance-enhanced multi-photon ionization (REMPI) has yielded information on the dissociation velocity distribution of the various breakup channels[22,23]. Structural probes such as ultrafast electron diffraction[24,25] are sensitive to the changing nuclear geometry but currently have insufficient temporal resolution to view vibrational dynamics and dissociation. Here we present structural measurements by ultrafast time-resolved X-ray scatter-
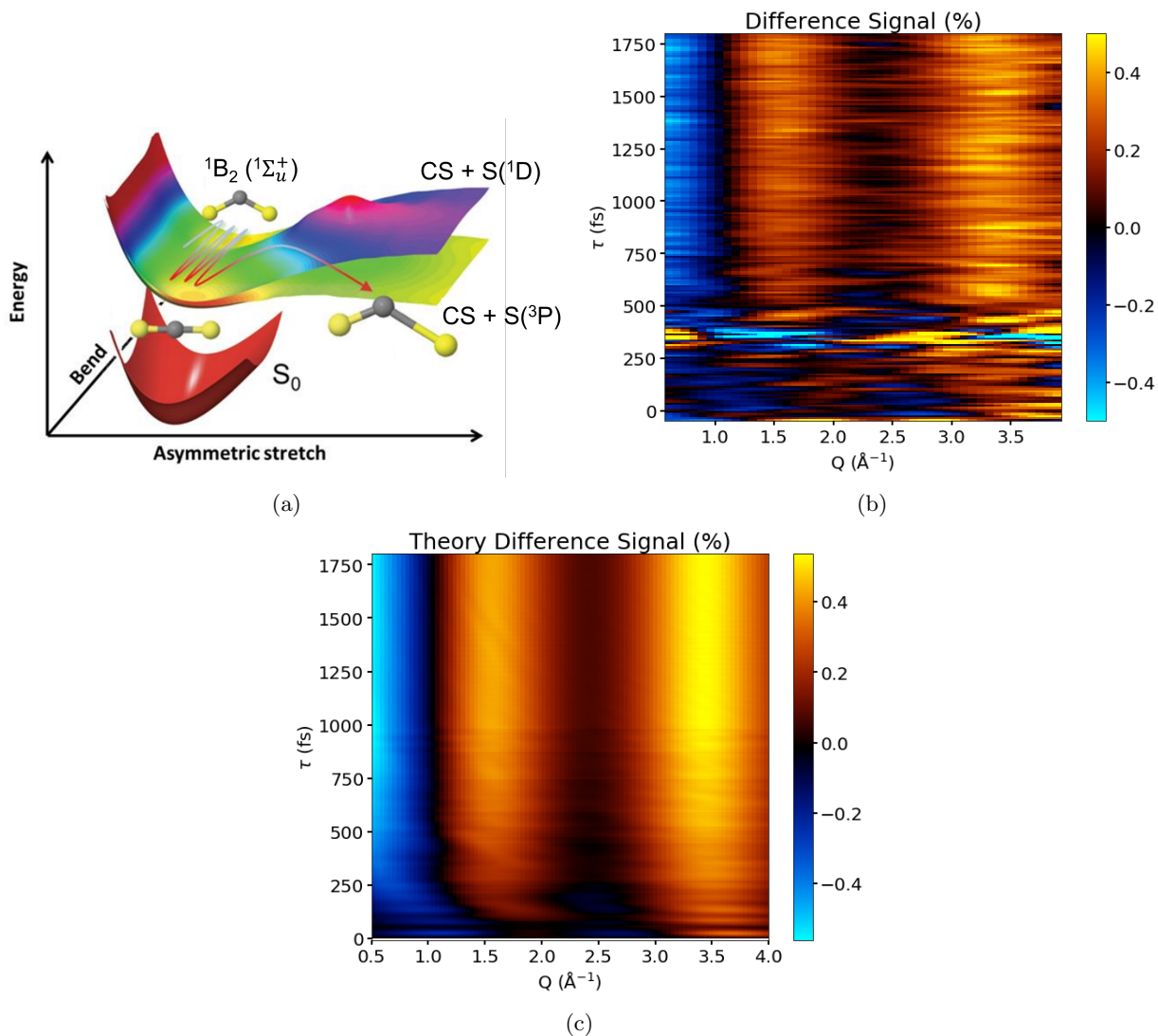
FIG. 1: Illustration of CS_2 reaction potential energy diagrams, dataset, and theoretical signal. (a) Representation of the potential energy surfaces for the states involved in this reaction. The ground-state (S_0) molecular geometry is linear, but the $^1B_2$ $\left(^1\Sigma_u^+\right)$ excited state has energy minima at bent geometries that induce molecular vibration along the bending coordinate. The nuclear wavepacket eventually couples to a manifold of dissociative states along the asymmetric stretch coordinate. (Figure adapted from Ref.[11].) (b) TRXS difference signal measured in our experiment. Q is the scattering vector momentum transfer in $\mathrm{\AA}^{-1}$ and τ is the UV pump-X-ray probe delay in femtoseconds. (c) Theoretical difference signal calculated from ensemble of surface-hopping trajectories (see Figure 3 and the Supplementary Material).

ing (TRXS) with sufficient time resolution to observe the vibrational dynamics and differentiate distinct dissociation channels.

TRXS is a well-proven technique for the measurement of the evolution of molecular structure in photochemical reactions[26–38]. In gas-phase TRXS experiments, a hard X-ray pulse probes the electron charge density distribution surrounding the nuclei following molecular photoexcitation. The pump-probe delay-dependent scattering pattern $S(Q, \tau)$ can be used to infer the evolution of the nuclear geometry. Time-domain analysis can distinguish between types of vibrational motion, quantify timescales of this motion, and support and validate calculations of molecular dynamics[30,33,39]. Frequency-resolved X-ray scattering (FRXS) provides an alternate view of TRXS data that facilitates the measurement of vibrational frequencies, dissociation velocities, and nuclear acceleration[26,27,32,40,41]. We employ both time- and frequency-domain techniques to extract information about the nuclear motion of UV-photoexcited CS_2.

II. EXPERIMENTAL DETAILS

Data were collected using X-ray scattering from UV-excited CS_2 molecules at the Coherent X-ray Imaging (CXI) instrument at the Linac Coherent Light Source (LCLS)[42]. The gas phase CS_2 sample flowed through a gas flow cell with a beryllium out-coupling window to minimize absorption and rescattering of scattered X-rays[29]. The sample was excited by a 200 nm, ~ 1 μJ, 80 fs full-width at half-maximum (FWHM) laser pulse. The sample was then probed by 9.8 keV (1.3 Å), 30 fs X-ray pulses generated by the LCLS instrument after a pump-probe delay τ.

The scattered X-rays were detected with a Jungfrau hard X-ray pixel detector with a pixel size of 75 μm, operating in a high-gain mode, situated approximately 8 cm behind the scattering cell. The raw detector images were thresholded to eliminate detector noise, and X-ray hits were then identified and localized within a 2×2 pixel area. The images were then corrected for the scattering geometry and for the variation of the Thomson scattering cross section with respect to the X-ray polarization[29]. The detector geometry was calibrated precisely by fitting a static scattering signal from sulfur hexafluoride (SF_6) to the expected scattering pattern, including both elastic and inelastic scattering effects[29].

Pump-probe data were recorded by varying the delay of the pump laser with respect to the X-rays. Individual shots taken in a pump-probe trace were then time binned with the use of an X-ray/laser cross-correlation time monitor, or "time tool," to correct for the jitter between the arrival time of the X-ray and the pump laser pulses[43]. The time tool was able to correct for the X-ray arrival timing jitter with a resolution of better than 10 fs. Approximately 18% of the shots were taken with the pump laser delayed by several nanoseconds to obtain the unpumped scattering signal $S_{\mathrm{off}}(Q)$ and used for background subtraction. Individual pump-probe shots were excluded if the X-ray pulse energy was below 20% of the mean as well as the quality of the time tool jitter correction fit. This excluded individual shots with technical issues, which amounted to about 14% of all pump-probe shots.

The time-resolved difference signal

$$\Delta S(Q, \tau) = \frac{S(Q, \tau) - S_{\mathrm{off}}(Q)}{S_{\mathrm{off}}(Q)} \qquad (1)$$

was obtained by sorting individual shots into 10 fs time bins and then integrating with respect to the azimuthal angle ϕ on the detector. The resulting time-resolved difference signal is shown in Figure 1b. The excitation fraction was estimated to be 1.4% by fitting the expected difference signal in Figure 1c to the experimental difference signal in Figure 1b. The number of shots varies across the time bins due to apparatus failure before the scan range could be filled uniformly, which accounts for the variation in noise across the time delay axis. In particular, the region between 300 and 400 fs in Figure 1b

contains very few shots (between 26 and 100 shots per time bin). This time delay region has large uncertainty and so is excluded from our time-resolved analysis. It is however included in our subsequent frequency analysis as this considers a much wider range of time delays, of which this region is a small subset.
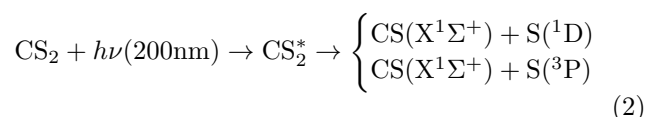
III. VIBRATIONAL DYNAMICS FOLLOWING PHOTOEXCITATION

Absorption of a 200 nm photon excites the CS_2 (X $^1\Sigma_g^+$) linear ground state (S_0 in Figure 1a) to a $^1\Sigma_u^+$ excited state. This excited state forms a potential energy surface that induces bending towards a $^1B_2$ symmetry and stretching towards $^1A'$ symmetry[44]. Subsequently, population may also transfer to one or more triplet potential surfaces via ISC, as shown schematically in Figure 1. In under a picosecond the molecule dissociates to a CS molecule and a sulfur atom in the ^3P or ^1D state. Comparison of the first 300 fs of motion in the excited CS_2 molecule projected from theoretical surface-hopping trajectories with the experimental data illuminates these initial structural changes.

A. Theoretical Signal

Molecular motion of CS_2 following photoexcitation at 200 nm was simulated using a trajectory surface-hopping code[17,45]. These simulations treat the nuclei as an ensemble of classical particles moving adiabatically on Born-Oppenheimer potential energy surfaces. Nonadiabatic[46] and spin-orbit interactions[3] are taken into account in regions of significant coupling by stochastically hopping between surfaces. In the simulations, the potential energy surfaces were calculated at the state-averaged CASSCF(10,8)/SVP level of theory using the electronic structure software MOLPRO[17,47]. The trajectories were propagated with the SHARC surface-hopping code[48] interfaced with the MOLPRO potential energies and couplings. Such trajectory ensembles for small-to moderately-sized molecules has been successfully employed to approximate the true behavior of the full molecular wavefunction[25,49,50].

Here, an ensemble of 213 distinct trajectories is propagated for a duration of 1 ps each. The trajectories are sampled from a ground-state Wigner distribution and then vertically excited to the $^1B_2$ $\left(^1\Sigma_u^+\right)$ state and allowed to evolve. This results in three families of product states: singlet and triplet dissociation of one of the sulfur atoms, along with a set of trajectories that remain bound up to 1 ps[17],
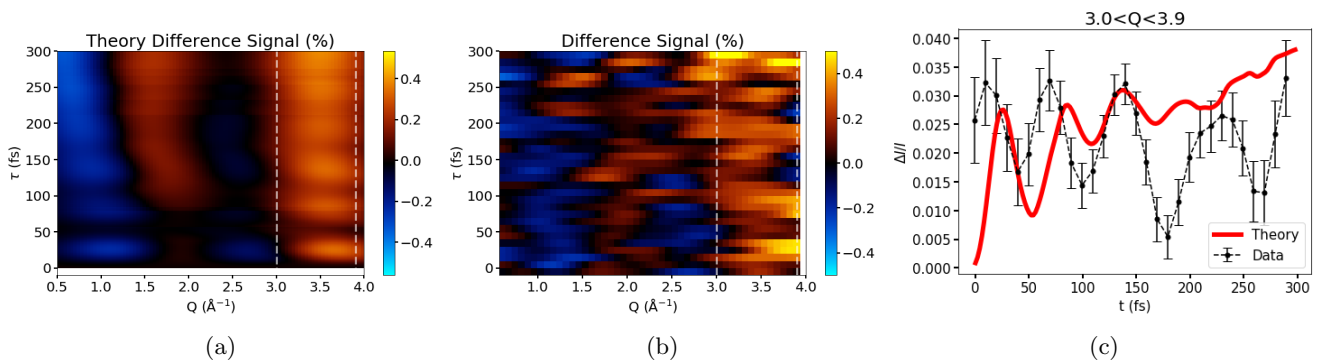
$$CS_2 + h\nu(200\mathrm{nm}) \rightarrow CS_2^* \rightarrow \begin{cases} CS(X^1\Sigma^+) + S(^1D) \\ CS(X^1\Sigma^+) + S(^3P) \end{cases}$$
$$(2)$$

FIG. 2: Time-resolved difference signal for the first 300 fs, azimuthally integrated and binned in Q and τ. (a) Predicted signal using the independent atom scattering model and an ensemble of 213 trajectories. (b) The experimental percent difference signal from Figure 1b, zoomed into first 300 fs. (c) Black points: Lineout of time-resolved difference signal between $3.0 < Q < 3.9$ Å^{-1} in (b). Red line: Corresponding lineout of theory in (a). The time alignment (x-axis) is the best fit of theory to data $\pm$ 6 fs. Dashed vertical lines in (a) and (b) indicate boundaries of the lineouts shown in (c).

Asymptotically, once a sulfur atom passes the dissociative limit ($R_{CS} \gg 3.4$ Å) in either the singlet or triplet state, the dissociation is propagated classically. Beyond 1 ps, the remaining bound trajectories are frozen in their final geometry.

Each individual trajectory represents one of the many possible pathways within an ensemble of quantum wave packets. Wave packet interference is specifically neglected, as each trajectory is presumed to move independently. The X-ray scattering for each trajectory is calculated with the rotationally averaged independent atom model (IAM)[29,51], which is given by

$$S_{\mathrm{IAM}}(Q) = \sum_{i,j}^{N_{\mathrm{at}}} f_i(Q) f_j(Q) \frac{\sin QR_{ij}}{QR_{ij}} + \sum_{i}^{N_{\mathrm{at}}} S_{\mathrm{inel},i}^{\mathrm{IAM}}(Q) \quad (3)$$

where $f_i(Q)$ is the scattering form factor of the ith atom, the i and j indices run over the atoms in the molecule, and R_{ij} is the distance between atoms i and j. The term $S_{\mathrm{inel},i}^{\mathrm{IAM}}(Q)$ represents all inelastic contributions to the scattering signal from each atom, i.e. Compton scattering. The time-dependent IAM scattering patterns for each trajectory are then added incoherently to obtain the full ensemble time-dependent scattering difference signal $\Delta S(Q, \tau)$, shown in Figure 1c.

B. Lineout Analysis

Comparison between the time-resolved data and the corresponding expected signal from the ensemble of trajectories can aid in confirming the presence of particular modes of motion. Bending and stretching motion in particular have distinct vibrational frequencies and appear as scattering signal in distinct regions of Q. The predominant initial motion in the trajectories is bending,

which appears most strongly as an oscillatory enhancement signal in the range $3.0 < Q < 3.9$ Å^{-1}, shown in Figure 2a. The corresponding experimental scattering difference signal is shown in Figure 2b.

The time of excitation ("time zero") was determined with an uncertainty of $\pm$6 fs by performing a nonlinear least squares fit between the full 2D theoretical and experimental time-resolved difference signals shown in Figure 2. Following this fit, we sum the difference signal in Q within the region mentioned above and plot the time-resolved integrated difference signal in Figure 2c. The corresponding lineout for the theoretical scattering signal is plotted alongside that for the data. The error bars on the data are obtained via bootstrapping[52] an uncertainty in each (Q, τ) bin and then adding time binned error bars in quadrature for the Q region lineout (see the Supplementary Material for bootstrap details).

Figure 2c shows the presence of oscillatory signal in the Q region associated with the initial bending of the molecule following photoexcitation. This signal is similar to the corresponding theoretical signal, exhibiting an oscillation in roughly the expected frequency and Q range for the predicted initial bending mode. Agreement is good for the first three oscillations between 0 and 150 fs and is best at 150 fs where the experimental error bars are smallest. Agreement between data and theory deteriorates following the third oscillation after 150 fs.

The fourth oscillation around 225 fs appears to be slowed significantly, indicating a change in the nature of the oscillation after 200 fs. A similar change in the phase and frequency of the vibration around the fourth oscillation may have been observed by Karashima et al. in previous time-resolved photoelectron spectroscopy measurements on photoexcited CS_2 (Ref.[18], Figure 3d). This change was not predicted by the exponentially decaying oscillation model in that work, nor by our 213-trajectory ensemble-averaged signal. This change in apparent fre-
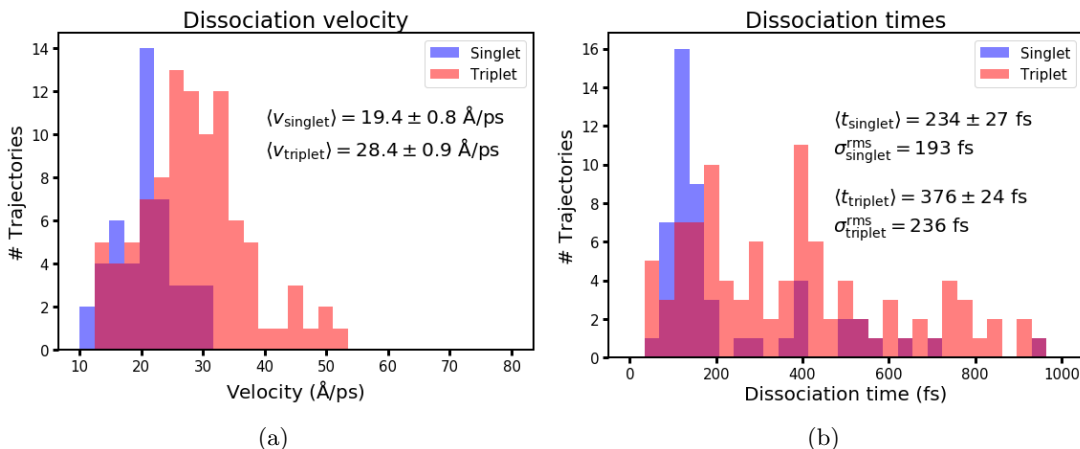
FIG. 3: Radial velocity and dissociation time histograms characterizing calculated singlet and triplet dissociation trajectories. Expectation values and associated uncertainties in these quantities for each channel are quoted in the figures. (a) Asymptotic dissociation radial velocity distributions for singlet and triplet channels. Singlets dissociate with lower mean velocity and narrower distribution than triplets. (b) Dissociation time distributions for singlet and triplet channels. Dissociation time is defined as time after photoexcitation until a trajectory passes the no-return carbon-sulfur bond distance of 3.4 Å. The singlet trajectories primarily reach the dissociation limit promptly within the first 200 fs, after which further singlet dissociation is suppressed. The triplet trajectories dissociate over a much broader time range. The rms spread in the dissociation times σ^{rms} is quoted in addition to the expectation value to illustrate the non-exponential behavior of the dissociation process.

quency could be explained by a quantum beat between the symmetric stretch (ν_1) and bending (ν_2) modes as shown in Ref.[18], Table 1.

IV. MOLECULAR FRAGMENTATION AND PRODUCT FORMATION

Following the initial vibrational motion launched by photoexcitation, vibrational mode coupling leads to dissociation of atomic sulfur in either a triplet or singlet state. The reaction dynamics of these competing channels cause them to play out on different timescales, and the energy distributions of the final states involved induce distinct dissociation velocity distributions. We use our ensemble of surface-hopping trajectories to predict the expected timescales and velocities of the singlet and triplet dissociation channels. The predicted velocity distributions are then compared to those extracted from the data to develop an understanding of the progression of the reaction dynamics with time.

A. Fragmentation Channels of CS_2

The singlet and triplet trajectories can be distinguished by the calculated distribution of their dissociation velocities as well as the times at which they occur. The velocity and dissociation time histograms for the singlet and triplet trajectories are shown in Figure 3. The singlet channel dissociates primarily within the first 200 fs, and the dissociation velocity distribution is narrow and peaked at 19.4 Å/ps. The triplet channel dissociates over a much wider range of times and produces a broader distribution of dissociation velocities that is peaked at 28.4 Å/ps. The partitioning of the remaining energy differs for the singlet and triplet channels as well, and is discussed further in the Supplementary Material. The mean time to dissociation $\langle t \rangle$ and the root mean square (rms) spread σ^{rms} of the distribution shown in Figure 3b do not coincide, as would be expected for a simple exponential decay model. This demonstrates that the dynamics governing the timescale to dissociation are more complicated than can be captured by a single intermediate state. These conclusions depart from previous studies[18] where a simple kinetic model for dissociation was employed.

The velocity distribution prediction has been verified in detail by experiments using a REMPI probe that are sensitive to the state of the dissociated sulfur atom[22]. In this work, it was shown that the $S(^1D)$ fragment emerges with a mean velocity of 11 Å/ps and a full width at half maximum (FWHM) of 5 Å/ps (see Figure 5.9 in Ref.[22]). This corresponds to a radial velocity of 19 Å/ps and a FWHM of 3.6 Å/ps, accounting for the recoil of the CS fragment. The sum of the three triplet state velocity distributions in[22] is much broader and peaked at 15.9 Å/ps with a FWHM of 14 Å/ps (see Figure 6.12 in Ref.[22]). This corresponds to a radial velocity distribution of 27.5 Å/ps and a FWHM of 22 Å/ps. These measured velocity distributions agree within error with the calculated distributions shown in Figure 3a.
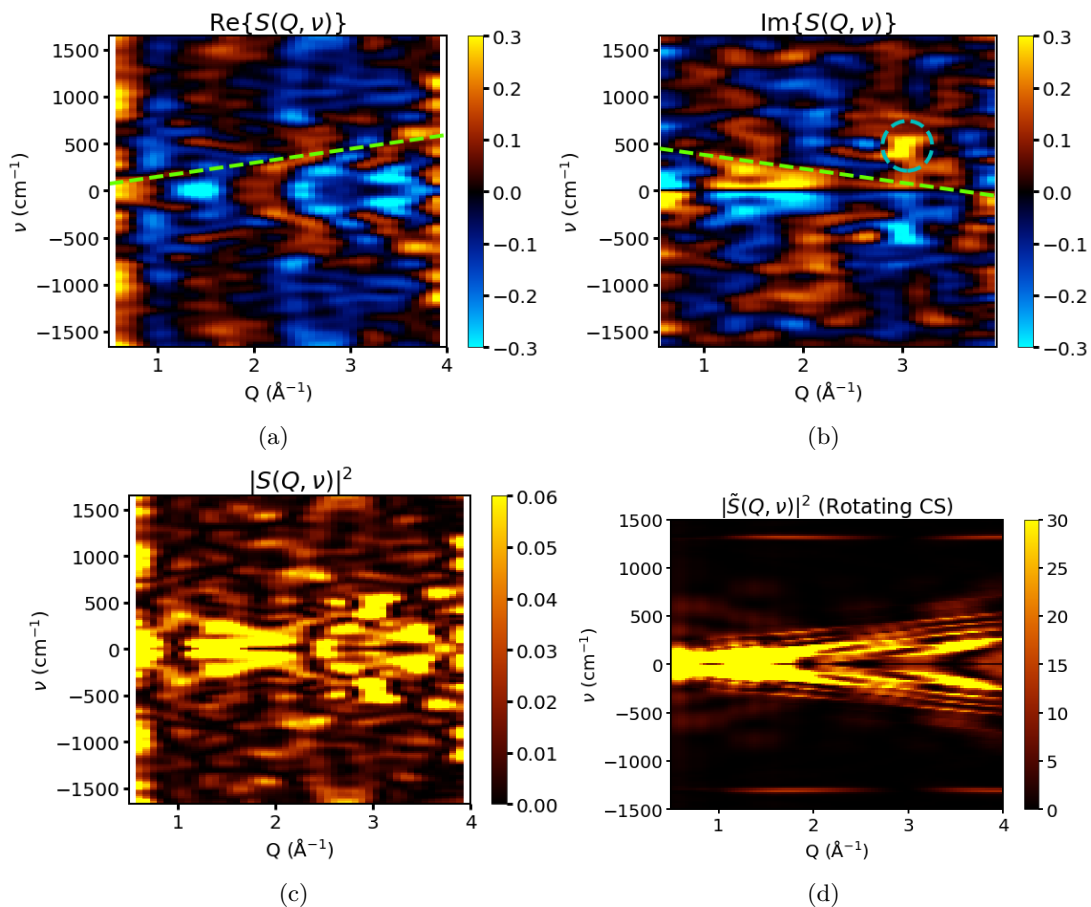
FIG. 4: FRXS representation of the TRXS data in the range $460 < \tau < 2260$ fs. (a) Real part of the FRXS data. There is a clear dissociation with a velocity of around 28 Å/ps, illustrated with a green dashed line. (b) Imaginary part of the FRXS data. The cyan circle illustrates a strong isolated signal at 500 cm^{-1}. The secondary dissociation line illustrated with green dashed line has same slope as line in Figure 4a. The negatively-sloped features may correspond to dissociation of atomic sulfur from a rovibrationally excited CS fragment. (c) Power spectrum of the FRXS data. The power spectrum is used in conjunction with a Hough transform in Section IV C to analyze the distribution of dissociation velocities. (d) FRXS power spectrum for a single characteristic trajectory with a CS fragment rotating at a frequency of 83 cm^{-1}. This plot illustrates the displacement of secondary dissociation lines by the frequency of the fragment rotation.

Estimates for the timescales of singlet and triplet dissociation have been provided by ultrafast photoelectron spectroscopy[11,18], but some ambiguity remains with respect to both the timescales and the mechanisms required for production of singlet and triplet atomic sulfur. Minns and coworkers suggested a model for dissociation that is consistent with our calculated dissociation times in Figure 3b[11,45]: singlet dissociation is suppressed after 200 fs, while the triplet channel continues to dissociate well past 500 fs. More recent work by Suzuki and coworkers[18] suggested a model that invoked a single intermediate state leading to both singlet and triplet dissociation, and measured nearly indistinguishable rise times for both products. TRXS can provide insight into the dissociation velocity distribution in distinct time ranges, thus providing a measure of the singlet/triplet production ratio as the reaction progresses.

B. Frequency-Resolved Analysis

To properly visualize the dissociation channels, we employ a family of techniques known as frequency-resolved X-ray scattering (FRXS). The FRXS representation of the data is obtained via a temporal Fourier transform (FT) of the time-resolved scattering signal

$$\tilde{S}(Q, \nu) = \mathcal{FT}_\tau \left\{ S(Q, \tau) \right\} \tag{4}$$

along the pump-probe delay axis τ. Molecular vibrations and dissociations are mapped to sparse and easily interpreted features in the FRXS representation[26,32,41]. Vibrations appear as horizontal lines centered at the vibrational frequency, with the phase of these lines giving information about the equilibrium bond distance of the vibration[41]. Dissociations appear as slanted lines in the

FRXS power spectrum $|S(Q,\nu)|^2$ where the radial dissociation velocity v corresponds to the slope of the line:[26] $\nu = Qv$. The phase of these dissociation lines gives information about the dissociation time shift[27,41] and the initial period of acceleration[32].

The FRXS representation of our data exhibits several of the signatures of dissociation that are expected from the theory trajectories. Figure 4 shows the FRXS representation of the data for a Fourier transform taken over the delay range $460 < \tau < 2260$ fs, the delay range with the best statistics in our data set. The FRXS data has been split into real part, imaginary part, and power spectrum to aid in visualizing the phases of the features as well as where they overlap in the power spectrum.

The real part of the Fourier transform (Figure 4a) displays a dissociation with a speed of ~ 28 Å/ps. The dashed green line is placed on the top half of the plot to aid in visualization of this dissociation signal. This dissociation speed is consistent with the theoretical mean triplet dissociation value of 28 ± 1 Å/ps (see Figure 3a) as well as prior measurements of the same process using a REMPI probe[22]. The consistency of the mean radial velocity with the predicted triplet radial velocity implies a lack of production of the lower-velocity singlet channel in this time. Although the previously dissociated singlet channel is also present in this time range, the most recently produced dissociations are always the most visible to FRXS since their scattering fringes still fall within the finite Q range of the detector. The visibility of dissociations generated prior to the start of the FT domain is suppressed by the fact that the scattering signal is concentrated at small scattering angles below our minimum Q value. The measurement of primarily triplet dissociations after 460 fs is thus also consistent with the prediction that the singlet channel is suppressed after 200 fs as shown in Figure 3b.

The imaginary part of the Fourier transform (Figure 4b) contains two signals of interest. First, there is an isolated island of signal well above the noise at $\nu = 500$ cm^{-1} and $Q = 3.0$ Å^{-1}, which is indicated with a cyan circle in the figure. This signal is spectrally broad and is centered at a frequency consistent with the initial bending motion following photoexcitation. The signal is furthermore located in the $3.0 < Q < 3.9$ Å^{-1} range that was illustrated with the lineout in Figure 2c and attributed to this initial motion. This could be evidence of the same vibrational beats between the ν_1 and ν_2 modes out past 1 ps measured in[18].

The imaginary part also exhibits negatively sloped lines that project back to $\nu = 500$ cm^{-1} at $Q = 0$. These appear to have a similar slope to the primary dissociation lines in Figure 4a, but they cannot be primary dissociation lines since the do not project back to $\nu_0 = 0$. Figure 4d illustrates a scenario in which these "secondary" dissociation lines can appear: atomic sulfur dissociation where the remaining CS fragment has been rovibrationally excited. The presence of a secondary dissociation line shifted by this amount indicates that there

could be rovibrational motion in the CS fragment with a period of around 63 fs. The magnitude of the frequency shift (~ 500 cm^{-1}) is inconsistent with the vibrational (1333 cm^{-1}) and rotational (84 cm^{-1}) frequencies of the CS radical (see the Supplementary Material). Since the presence of a potential secondary dissociation line cannot be adequately explained by vibrational or rotational motion in the CS fragment, we simply note its apparent presence here.

Visualization of a dissociation process with a wide velocity distribution using FRXS is challenging because the dissociation features in $\tilde{S}(Q,\nu)$ must be seen by eye. In our case, while we see evidence for dissociation of atomic sulfur centered at around 28 Å/ps, we cannot conclude anything quantitative about the velocity distribution from Figure 4 alone. We now turn to the Hough transform in order to quantitatively characterize the measured dissociation velocity distributions.

C. Velocity Distribution Extraction: Hough Transform

The Hough transform $H(v,\nu_0)$ is a slope- and intercept-resolved integral transform of the power spectrum of the FRXS data[53,54]. It is defined as follows

$$C_{v,\nu_0} : \nu = \nu_0 + Qv$$
$$H(v,\nu_0) = \oint_{C_{v,\nu_0}} |S(Q,\nu)|^2 dQd\nu \qquad (5)$$

where C_{v,ν_0} is a line in (Q,ν) space over which the line integral of the power spectrum is computed, v is the slope of the line in (Q,ν) space corresponding to the dissociation velocity, and ν_0 is the y-intercept of the line in (Q,ν) space projected back to $Q = 0$.

The Hough transform maps bright lines from an input image to bright points in the transformed representation. Any primary dissociation lines with slope v present in the FRXS plot will therefore manifest as bright points in the Hough transform along the $\nu_0 = 0$ axis. Likewise, any secondary dissociation lines will manifest at the same slope v and a nonzero ν_0. In this fashion, the Hough transform allows us to quantitatively compare the strength of the various dissociation lines present in an FRXS plot even in the presence of noise due to its sparse representation of the dissociation lines.

We applied the Hough transform to the FRXS data for Fourier transforms taken over two distinct time delay ranges, $0 < \tau < 600$ fs and $1400 < \tau < 2000$ fs, in the region $Q < 3$ Å^{-1}. This range was needed to provide sufficient scattering statistics for our analysis, particularly in the earlier time bin. In addition, the 600 fs time window provides a sufficiently large time domain for FRXS representations suitable for applying the Hough transform. Meanwhile, restricting the Q range improves the fidelity of the Hough transform by excluding a regime in which the noise level becomes large enough to pollute the results. Taking a lineout of the Hough transform along
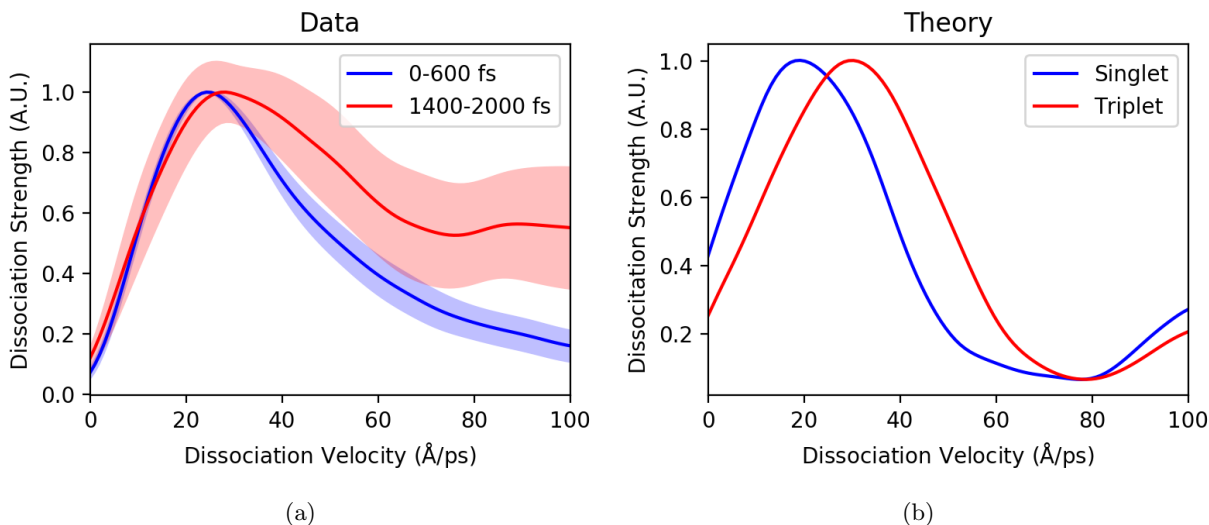
FIG. 5: Hough transform feature strength plots for data and theory. (a) Velocity-resolved Hough transform feature strength in our time-resolved data over a range of dissociation velocities for two separate time delay regions. Hough transform lineout is taken for y-intercept $\nu_0 = 0$. The legend indicates the time delays over which the Fourier transform for the Hough transform lineout is taken. The shaded region indicates the bootstrapped errorbar of the Hough transform. The early-time transform (blue curve) shows a sharply peaked distribution around 24 Å/ps, consistent with a mixture composed of the singlet and triplet channels. The late-time transform (red curve) shows a much broader distribution of dissociation velocities and a maximum at higher velocity of 28 Å/ps, consistent with the expected velocity distribution of the triplet channel. (b) Theoretical velocity-resolved Hough transform feature strength for ensembles of singlet and triplet trajectories. These distributions peak at 19 Å/ps and 30 Å/ps, respectively.

the $\nu_0 = 0$ axis shows the relative strength of dissociation lines with particular velocities in the FRXS data. This yields the plot shown in Figure 5a. For both time delay ranges, there is a signal strength maximum between 20 and 30 Å/ps, indicating the presence of dissociations with this velocity in the data. The shaded regions around both curves represent the uncertainty obtained by bootstrapping, where the bootstrap re-sampling was taken over individual X-ray shots. See the Supplementary Material for further details on our bootstrap method.

The Hough transforms across these two distinct time ranges contrasts the dominant dissociation velocities that occur at each time. For the early-time data (0-600 fs), there is a maximum at 24 Å/ps with a relatively small uncertainty and peak width. For the late-time data (1400-2000 fs), the Hough transform is both broader and peaked at a higher dissociation velocity of 28 Å/ps. Taken together, these two curves demonstrate that as the reaction time progresses, CS_2 tends to dissociate with progressively higher dissociation velocity and broader distribution.

A comparison with the Hough transforms of the simulated singlet and triplet trajectories yields information about the relative strengths of singlet and triplet dissociation at each reaction time range. The Hough transforms of the simulated singlet and triplet trajectory data are shown in Figure 5b. The singlet curve is peaked at 21 Å/ps, while the triplet curve is peaked at 28 Å/ps

with a slightly broader velocity distribution. The Hough transform of our data in Figure 5a can thus be interpreted as follows. In the first 600 fs, CS_2 dissociates into a mixture of singlet and triplet sulfur in apparently roughly equal quantities. Beyond 1400 fs, the dissociation that occurs is primarily triplet in nature.

The velocity distribution measurements can provide some extra evidence for resolving the discrepancy between the models for dissociation proposed in[11] and[18]. The analysis in[18] suggested that both singlet and triplet dissociation channels proceed from either a single intermediate state, or else from two distinct intermediate states whose time dependence is indistinguishable. In such a situation the ratio of singlet to triplet dissociation should remain constant over time. We should therefore observe a time-independent velocity distribution in the Hough transform. In our analysis we clearly see a change in velocity distribution with time which, due to the different velocity distributions associated with the two fragment channels, is indicative of a change in branching ratio towards a higher relative yield of triplet product states as the pump-probe delay increases.

The observation of a changing velocity distribution is consistent with the earlier work of[11] as well as the trajectory calculations used here. In both cases, the suggestion is that after excitation the branching space is defined by competition between singlet dissociation and IC processes that trap population in the excited singlet

manifold by relatively large barriers to dissociation. This trapping suppresses further singlet dissociation after the first few hundred femtoseconds following excitation. The trapped bound singlet state population can then undergo ISC which transfers population into the triplet manifold, leading to the formation of the triplet state dissociation fragments over an extended period of time. Such dynamics would lead to a change in the observed velocity distributions as a function of the time as the relative importance of the triplet state dissociation trajectories in the measured velocity distribution increases with delay. Our measurements and analysis suggest that the dissociation velocity distribution shifts from being a mixture of singlet and triplet state dissociation in the first 600 fs, to being dominated by the triplet state dissociation after 1400 fs. In this sense, our data are more consistent with the model suggested by Minns and coworkers[11] than the one suggested by Suzuki and coworkers[18].

V. CONCLUSION

We performed time-resolved pump-probe X-ray scattering in gas-phase photoexcited CS_2 at the CXI instrument at LCLS with the aim of measuring the coherent nuclear motion that ensues. We observe strong evidence for the expected bending motion following photoexcitation at early time delays. We also observe signals at late time delays that are consistent with atomic sulfur dissociation into both singlet and triplet channels.

The observation of the bending mode that is initially excited shows reasonable agreement with theory and shares some similarities with previously reported photoelectron spectroscopy data. The vibrational frequency decreases around the fourth oscillation, indicating a change in the nature of the excited vibrational mode. This change in frequency could be evidence for the vibrational mode coupling that is necessary to achieve the observed dissociation products. A comparison of the depth of oscillation in the data and theory suggests that the theory trajectories may underestimate the degree of vibrational coherence that is maintained beyond the third oscillation.

The observed dissociation velocity distributions are consistent with previous work on CS_2. By utilizing the Hough transform to extract the slopes of the dominant features in the FRXS plot, we are able to observe the distribution of dissociation radial velocities at early and late time delays. The first 600 fs show strong evidence for a mixture of singlet and triplet dissociation, while later time delays between 1400 and 2000 fs show a broader distribution consistent with the expected dominant triplet dissociation channel. Our radial velocity distribution measurements and calculated trajectories support a multi-state model for the reaction pathways to singlet and triplet sulfur dissociation[11]. This style of analysis, which relies on the experimental data alone, can be used to characterize weak dissociation signals using TRXS.

[1] M. S. Schuurman and A. Stolow, "Dynamics at Conical Intersections," Annual Review of Physical Chemistry **69**, 427–450 (2018), _eprint: https://doi.org/10.1146/annurev-physchem-052516-050721.

[2] W. Siebrand and M. Z. Zgierski, en"Matrix elements for intersystem crossing," Chemical Physics Letters **35**, 151–155 (1975).

[3] S. Mai, P. Marquetand, and L. González, en"A general method to describe intersystem crossing dynamics in trajectory surface hopping," International Journal of Quantum Chemistry **115**, 1215–1231 (2015), _eprint: https://onlinelibrary.wiley.com/doi/pdf/10.1002/qua.24891.

[4] S. Mai, P. Marquetand, and L. González, en"Nonadiabatic dynamics: The SHARC approach," WIREs Computational Molecular Science **8**, e1370 (2018), _eprint: https://onlinelibrary.wiley.com/doi/pdf/10.1002/wcms.1370.

[5] M. E. Corrales, V. Loriot, G. Balerdi, J. González-Vázquez, R. d. Nalda, L. Bañares, and A. H. Zewail, en"Structural dynamics effects on the ultrafast chemical bond cleavage of a photodissociation reaction," Physical Chemistry Chemical Physics **16**, 8812–8818 (2014), publisher: Royal Society of Chemistry.

[6] K. F. Chang, H. Wang, S. M. Poullain, D. Prendergast, D. M. Neumark, and S. R. Leone, "Mapping wave packet bifurcation at a conical intersection in CH3I by attosecond XUV transient absorption spectroscopy," The Journal of Chemical Physics **154**, 234301 (2021), publisher: American Institute of Physics.

[7] K. F. Chang, M. Reduzzi, H. Wang, S. M. Poullain, Y. Kobayashi, L. Barreau, D. Prendergast, D. M. Neumark, and S. R. Leone, en"Revealing electronic state-switching at conical intersections in alkyl iodides by ultrafast XUV transient absorption spectroscopy," Nature Communications **11**, 4042 (2020),

bandiera_abtest: a Cc_license_type: cc_by Cg_type: Nature Research Journals Number: 1 Primary_atype: Research Publisher: Nature Publishing Group Subject_term: Chemistry;Physics Subject_term_id: chemistry;physics.

[8] S. Matsika, "Radiationless Decay of Excited States of Uracil through Conical Intersections," The Journal of Physical Chemistry A **108**, 7584–7590 (2004), publisher: American Chemical Society.

[9] S. Perun, A. L. Sobolewski, and W. Domcke, "Conical Intersections in Thymine," The Journal of Physical Chemistry A **110**, 13238–13244 (2006), publisher: American Chemical Society.

[10] C. Starrs, M. N. Jego, A. Mank, and J. W. Hepburn, en"Mode specific photodissociation of the 1B2 state of carbon disulfide," The Journal of Physical Chemistry **96**, 6526–6529 (1992).

[11] A. D. Smith, E. M. Warne, D. Bellshaw, D. A. Horke, M. Tudorovskya, E. Springate, A. J. H. Jones, C. Cacho, R. T. Chapman, A. Kirrander, and R. S. Minns, "Mapping the Complete Reaction Path of a Complex Photochemical Reaction," Physical Review Letters **120**, 183003 (2018), publisher: American Physical Society.

[12] C. Z. Bisgaard, O. J. Clarkin, G. Wu, A. M. D. Lee, O. Geßner, C. C. Hayden, and A. Stolow, "Time-Resolved Molecular Frame Dynamics of Fixed-in-Space CS2 Molecules," Science **323**, 1464–1468 (2009), publisher: American Association for the Advancement of Science.

[13] P. Hockett, C. Z. Bisgaard, O. J. Clarkin, and A. Stolow, en"Time-resolved imaging of purely valence-electron dynamics during a chemical reaction," Nature Physics **7**, 612–615 (2011), number: 8 Publisher: Nature Publishing Group.

[14] D. Townsend, H. Satzger, T. Ejdrup, A. M. D. Lee, H. Stapelfeldt, and A. Stolow, "B21(σu+1) excited state decay dynamics in CS2," The Journal of Chemical Physics **125**, 234302 (2006), publisher: American Institute of Physics.

[15] P. Farmanara, O. Steinkellner, M. T. Wick, M. Wittmann, G. Korn, V. Stert, and W. Radloff, "Ultrafast internal conversion and photodissociation of molecules excited by femtosecond 155 nm laser pulses," The Journal of Chemical Physics **111**, 6264–6270 (1999), publisher: American Institute of Physics.

[16] P. Farmanara, V. Stert, and W. Radloff, "Ultrafast predissociation and coherent phenomena in CS2 excited by femtosecond laser pulses at 194–207 nm," The Journal of Chemical Physics **111**, 5338–5343 (1999), publisher: American Institute of Physics.

[17] D. Bellshaw, D. A. Horke, A. D. Smith, H. M. Watts, E. Jager, E. Springate, O. Alexander, C. Cacho, R. T. Chapman, A. Kirrander, and R. S. Minns, en"Ab-initio surface hopping and multiphoton ionisation study of the photodissociation dynamics of CS2," Chemical Physics Letters Ahmed Zewail (1946-2016) Commemoration Issue of Chemical Physics Letters, **683**, 383–388 (2017).

[18] S. Karashima, Y.-I. Suzuki, and T. Suzuki, "Ultrafast Extreme Ultraviolet Photoelectron Spectroscopy of Nonadiabatic Photodissociation of CS2 from 1B2 (1Σu+) State: Product Formation via an Intermediate Electronic State," The Journal of Physical Chemistry Letters **12**, 3755–3761 (2021), publisher: American Chemical Society.

[19] E. M. Warne, A. D. Smith, D. A. Horke, E. Springate, A. J. H. Jones, C. Cacho, R. T. Chapman, and R. S. Minns, "Time resolved detection of the S(1D) product of the UV induced dissociation of CS2," The Journal of Chemical Physics **154**, 034302 (2021), publisher: American Institute of Physics.

[20] R. Spesyvtsev, T. Horio, Y.-I. Suzuki, and T. Suzuki, "Observation of the wavepacket dynamics on the 1B2(1Σu+) state of CS2 by sub-20 fs photoelectron imaging using 159 nm probe pulses," The Journal of Chemical Physics **142**, 074308 (2015), publisher: American Institute of Physics.

[21] T. Horio, R. Spesyvtsev, Y. Furumido, and T. Suzuki, "Real-time detection of S(1D2) photofragments produced from the 1B2(1Σu+) state of CS2 by vacuum ultraviolet photoelectron imaging using 133 nm probe pulses," The Journal of Chemical Physics **147**, 013932 (2017), publisher: American Institute of Physics.

[22] E. Campbell, *Atomic polarisation in molecular photodissociation*, PhD Thesis, University of Oxford (2016).

[23] M. Brouard, E. K. Campbell, R. Cireasa, A. J. Johnsen, and W.-H. Yuen, "The ultraviolet photodissociation of CS2: The S(1D2) channel," The Journal of Chemical Physics **136**, 044310 (2012), publisher: American Institute of Physics.

[24] M. Stefanou, K. Saita, D. V. Shalashilin, and A. Kirrander, en"Comparison of ultrafast electron and X-ray diffraction – A computational study," Chemical Physics Letters Ahmed Zewail (1946-2016) Commemoration Issue of Chemical Physics Letters, **683**, 300–305 (2017).

[25] W. O. Razmus, K. Acheson, P. Bucksbaum, M. Centurion, E. Champenois, I. Gabalski, M. C. Hoffman, A. Howard, M.-F. Lin, Y. Liu, P. Nunes, S. Saha, X. Shen, M. Ware, E. M. Warne, T. Weinacht, K. Wilkin, J. Yang, T. J. A. Wolf, A. Kirrander, R. S. Minns, and R. Forbes, en"Multichannel photodissociation dynamics in CS 2 studied by ultrafast electron diffraction," Physical Chemistry Chemical Physics (2022), 10.1039/D2CP01268E, publisher: Royal Society of Chemistry.

[26] M. R. Ware, J. M. Glownia, N. Al-Sayyad, J. T. O'Neal, and P. H. Bucksbaum, "Characterizing dissociative motion in time-resolved x-ray scattering from gas-phase diatomic molecules," Physical Review A **100**, 033413 (2019), publisher: American Physical Society.

[27] M. R. Ware, *From {Time}-resolved to {Frequency}-resolved {X}-ray {Scattering}*, Ph.D. thesis, Stanford University (2019).

[28] B. Stankus, H. Yong, N. Zotev, J. M. Ruddock, D. Bellshaw, T. J. Lane, M. Liang, S. Boutet, S. Carbajo, J. S. Robinson, W. Du, N. Goff, Y. Chang, J. E. Koglin, M. P. Minitti, A. Kirrander, and P. M. Weber, en"Ultrafast X-ray scattering reveals vibrational coherence following Rydberg excitation," Nature Chemistry **11**, 716–721 (2019), bandiera_abtest: a Cg_type: Nature Research Journals Number: 8 Primary_atype: Research Publisher: Nature Publishing Group Subject_term: Chemical physics;Excited states;Reaction kinetics and dynamics Subject_term_id: chemical-physics;excited-states;kinetics-and-dynamics.

[29] B. Stankus, H. Yong, J. Ruddock, L. Ma, A. M. Carrascosa, N. Goff, S. Boutet, X. Xu, N. Zotev, A. Kirrander, M. P. Minitti, and P. M. Weber, en"Advances in ultrafast gas-phase x-ray scattering," Journal of Physics B: Atomic, Molecular and Optical Physics **53**, 234004 (2020), publisher: IOP Publishing.

[30] M. P. Minitti, J. M. Budarz, A. Kirrander, J. S. Robinson, J. M. Glownia, M. Kozina, H. T. Lemke, M. Sikorski, Y. Feng, S. Nelson, K. Saita, B. Stankus, T. Northey, J. B. Hastings, and P. M. Weber, "Imaging Molecular Motion: Femtosecond X-Ray Scattering of an Electrocyclic Chemical Reaction," Physical Review Letters **114**, 255501 (2015), publisher: American Physical Society.

[31] J. M. Budarz, M. P. Minitti, D. V. Cofer-Shabica, B. Stankus, A. Kirrander, J. B. Hastings, and P. M. Weber, en"Observation of femtosecond molecular dynamics via pump–probe gas phase x-ray scattering," Journal of Physics B: Atomic, Molecular and Optical Physics **49**, 034001 (2016), publisher: IOP Publishing.

[32] I. Gabalski, M. R. Ware, and P. H. Bucksbaum, en"X-ray scattering signatures of early-time accelerations in iodine dissociation," Journal of Physics B: Atomic, Molecular and Optical Physics **53**, 244002 (2020), publisher: IOP Publishing.

[33] H. Yong, A. M. Carrascosa, L. Ma, B. Stankus, M. P. Minitti, A. Kirrander, and P. M. Weber, en"Determination of excited state molecular structures from time-resolved gas-phase X-ray scattering," Faraday Discussions **228**, 104–122 (2021), publisher: The Royal Society of Chemistry.

[34] H. Yong, X. Xu, J. M. Ruddock, B. Stankus, A. M. Carrascosa, N. Zotev, D. Bellshaw, W. Du, N. Goff, Y. Chang, S. Boutet, S. Carbajo, J. E. Koglin, M. Liang, J. S. Robinson, A. Kirrander, M. P. Minitti, and P. M. Weber, "Ultrafast X-ray scattering offers a structural view of excited-state charge transfer," Proceedings of the National Academy of Sciences **118**, e2021714118

(2021), publisher: Proceedings of the National Academy of Sciences.

[35] G. Dixit, O. Vendrell, and R. Santra, en"Imaging electronic quantum motion with light," Proceedings of the National Academy of Sciences **109**, 11636–11640 (2012), publisher: National Academy of Sciences Section: Physical Sciences.

[36] G. Dixit, J. M. Slowik, and R. Santra, "Theory of time-resolved nonresonant x-ray scattering for imaging ultrafast coherent electron motion," Physical Review A **89**, 043409 (2014), publisher: American Physical Society.

[37] G. Dixit and R. Santra, "Time-resolved ultrafast x-ray scattering from an incoherent electronic mixture," Physical Review A **96**, 053413 (2017), publisher: American Physical Society.

[38] T. Bredtmann, M. Ivanov, and G. Dixit, en"X-ray imaging of chemically active valence electrons during a pericyclic reaction," Nature Communications **5**, 5589 (2014), number: 1 Publisher: Nature Publishing Group.

[39] H. Yong, N. Zotev, J. M. Ruddock, B. Stankus, M. Simmermacher, A. M. Carrascosa, W. Du, N. Goff, Y. Chang, D. Bellshaw, M. Liang, S. Carbajo, J. E. Koglin, J. S. Robinson, S. Boutet, M. P. Minitti, A. Kirrander, and P. M. Weber, en"Observation of the molecular response to light upon photoexcitation," Nature Communications **11**, 2157 (2020), bandiera_abtest: a Cc_license_type: cc_by Cg_type: Nature Research Journals Number: 1 Primary_atype: Research Publisher: Nature Publishing Group Subject_term: Chemical physics;Excited states;Imaging techniques;Quantum chemistry Subject_term_id: chemical-physics;excited-states;imaging-techniques;quantum-chemistry.

[40] M. R. Ware, J. M. Glownia, A. Natan, J. P. Cryan, and P. H. Bucksbaum, "On the limits of observing motion in time-resolved X-ray scattering," Philosophical Transactions of the Royal Society A: Mathematical, Physical and Engineering Sciences **377**, 20170477 (2019), publisher: Royal Society.

[41] P. H. Bucksbaum, M. R. Ware, A. Natan, J. P. Cryan, and J. M. Glownia, "Characterizing Multiphoton Excitation Using Time-Resolved X-ray Scattering," Physical Review X **10**, 011065 (2020), publisher: American Physical Society.

[42] S. Boutet and G. J. Williams, en"The Coherent X-ray Imaging (CXI) instrument at the Linac Coherent Light Source (LCLS)," New Journal of Physics **12**, 035024 (2010), publisher: IOP Publishing.

[43] M. Harmand, R. Coffee, M. R. Bionta, M. Chollet, D. French, D. Zhu, D. M. Fritz, H. T. Lemke, N. Medvedev, B. Ziaja, S. Toleikis, and M. Cammarata, en"Achieving few-femtosecond time-sorting at hard X-ray free-electron lasers," Nature Photonics **7**, 215–218 (2013), number: 3 Publisher: Nature Publishing Group.

[44] R. R. Sadeghi, S. R. Gwaltney, J. L. Krause, R. T. Skodje, and P. M. Weber, "Structure and dynamics of the S3 state of CS2," The Journal of Chemical Physics **107**, 6570–6576 (1997), publisher: American Institute of Physics.

[45] D. Bellshaw, R. S. Minns, and A. Kirrander, en"Correspondence between electronic structure calculations and simulations: nonadiabatic dynamics in CS 2," Physical Chemistry Chemical Physics **21**, 14226–14237 (2019), publisher: Royal Society of Chemistry.

[46] M. Richter, P. Marquetand, J. González-Vázquez, I. Sola, and L. González, "SHARC: ab Initio Molecular Dynamics with Surface Hopping in the Adiabatic Representation Including Arbitrary Couplings," Journal of Chemical Theory and Computation **7**, 1253–1258 (2011), publisher: American Chemical Society.

[47] H.-J. Werner, P. J. Knowles, G. Knizia, F. R. Manby, and M. Schütz, en"Molpro: a general-purpose quantum chemistry program package," WIREs Computational Molecular Science **2**, 242–253 (2012), _eprint: https://onlinelibrary.wiley.com/doi/pdf/10.1002/wcms.82.

[48] S. Mai, M. Richter, M. Heindl, M. F. S. J. Menger, A. Atkins, M. Ruckenbauer, F. Plasser, L. M. Ibele, S. Kropf, M. Oppel, P. Marquetand, and L. Gonz\'alez, "SHARC2.1: Surface Hopping Including Arbitrary Couplings — Program Package for Non-Adiabatic Dynamics," (2019), published: sharc-md.org.

[49] M. D. Hack, A. M. Wensmann, D. G. Truhlar, M. Ben-Nun, and T. J. Martinez, "Comparison of full multiple spawning, trajectory surface hopping, and converged quantum mechanics for electronically nonadiabatic dynamics," The Journal of Chemical Physics **115**, 1172–1186 (2001), publisher: American Institute of Physics.

[50] A. Kirrander, K. Saita, and D. V. Shalashilin, "Ultrafast X-ray Scattering from Molecules," Journal of Chemical Theory and Computation **12**, 957–967 (2016), publisher: American Chemical Society.

[51] A. Moreno Carrascosa, H. Yong, D. L. Crittenden, P. M. Weber, and A. Kirrander, "Ab Initio Calculation of Total X-ray Scattering from Molecules," Journal of Chemical Theory and Computation **15**, 2836–2846 (2019), publisher: American Chemical Society.

[52] B. Efron and R. Tibshirani, en"The Bootstrap Method for Assessing Statistical Accuracy," Behaviormetrika **12**, 1–35 (1985).

[53] R. O. Duda and P. E. Hart, "Use of the Hough transformation to detect lines and curves in pictures," Communications of the ACM **15**, 11–15 (1972).

[54] P. E. Hart, "How the Hough transform was invented [DSP History]," IEEE Signal Processing Magazine **26**, 18–22 (2009), conference Name: IEEE Signal Processing Magazine.